Eur. Phys. J. C 9, 623–631 (1999)
DOI 10.1007/s100529900037

THE EUROPEAN PHYSICAL JOURNAL C

The additive quark model revisited: Hadron- and photon-induced cross sections

P. Desgrolard[1,a], M. Giffon[1,b], E. Martynov[2,c], E. Predazzi[3,d]

[1] Institut de Physique Nucléaire de Lyon, IN2P3-CNRS et Université Claude Bernard, 43 boulevard du 11 novembre 1918, F-69622 Villeurbanne Cedex, France
[2] Bogoliubov Institute for Theoretical Physics, NAS of Ukraine, Metrologicheskaja 14b, 252143, Kiev-143, Ukraine
[3] Dipartimento di Fisica Teorica – Università di Torino and Sezione INFN di Torino, Italy

Received: 23 November 1998 / Revised version: 18 December 1998 / Published online: 30 June 1999

Abstract. The standard additive quark model and the ensuing counting rules are modified to take into account not only the quark–gluonic content of the Pomeron but also of the secondary Reggeons, as well as the fact that the soft Pomeron is not just a gluonic ladder. A much-improved description of pp, πp, γp and $\gamma\gamma$ cross sections is obtained.

1 Introduction

The additive quark model (AQM)[1–4] has provided for a long time a simple and successful model to describe, in particular, the main relations between the high-energy cross sections of different hadronic processes [5,6]. Considering, for example, the pion–nucleon and the nucleon–nucleon interactions, one finds that the relation $\sigma_{\rm tot}^{\pi N}/\sigma_{\rm tot}^{NN} = 2/3$ is in agreement with the available experimental data within an accuracy of a few percent. A linear dependence of the amplitudes on the number of quarks inside the scattered hadrons has been confirmed on more fundamental grounds through QCD-like models [7,8].

A new, interesting case to which we can apply (and test) the AQM involves extending it to photon-induced reactions, because the data on these processes are now available up to quite high energies ($\sqrt{s} \approx 200\,\mathrm{GeV}$ for γp and $\sqrt{s} \approx 100$ GeV for $\gamma\gamma$ inelastic cross sections) [9,10]. The three processes pp, γp and $\gamma\gamma$ are related via unitarity and factorization, and this is the only complete set of related processes for which we have data. For the set of pp, πp, $\pi\pi$ reactions, for instance, the data on $\pi\pi$ interactions are in fact absent, and πp total cross sections are known only up to relatively low energies ($\sqrt{s} < 30\,\mathrm{GeV}$).

Considering the above-mentioned γp processes, we show that the standard AQM does not describe the data with sufficiently high quality [1]. In Sect. 3, we propose a modified AQM that takes into account the quark–gluonic content of the exchanged Reggeons and the corrections to the Pomeron–quark interaction. As a first try, we discuss the cases of the Pomeron and f Reggeon, because they contribute to all amplitudes. The suggested modification provides a much-improved agreement with the experimental data. In order to make clear the content of our modification, we will not consider here the scattering processes at $t \neq 0$. The parameterization of the scattering amplitudes at $t \neq 0$ is much more complex than at $t = 0$. This will be the subject of a forthcoming paper.

[a] e-mail: desgrolard@ipnl.in2p3.fr
[b] e-mail: giffon@ipnl.in2p3.fr
[c] e-mail: martynov@bitp.kiev.ua
[d] e-mail: predazzi@to.infn.it

[1] We cannot compare the quality of our fit with those presented in some recent papers [11,12] because their χ^2 are not given. Differences between their and our predictions for cross sections at higher energies are discussed in Sect. 4.

2 The old additive quark model

2.1 The Pomeron

The traditional additive quark model treats the elastic scattering of two hadrons at high energy as a Pomeron exchange between two quarks, one in each hadron. From the point of view of the quark–gluon picture, the Pomeron is represented by a gluon ladder where end-points are coupled with quark lines. The simplest diagram describing the main contribution to elastic hadron–hadron amplitude in the old AQM is exemplified in Fig. 1.

In accordance with the AQM, when two hadrons h_1 and h_2 collide, and they are made of n_1 and n_2 quarks, respectively, the Pomeron contribution to the elastic amplitude has the form

$$A_{\mathcal{P}}^{(h_1h_2)}(s,t) = n_1 n_2 P_{h_1} P_{h_2} A_{\mathcal{P}}^{(qq)}(s_{h_1h_2},t) G_{\mathcal{P}}^{(h_1)}(t) G_{\mathcal{P}}^{(h_2)}(t), \quad (1)$$

where $\sqrt{P_{h_i}}$ is the probability of finding the hadron h_i as a quark system, $A_{\mathcal{P}}^{(qq)}(s,t)$ is the amplitude of elastic scattering of quarks due to the Pomeron, and the squared

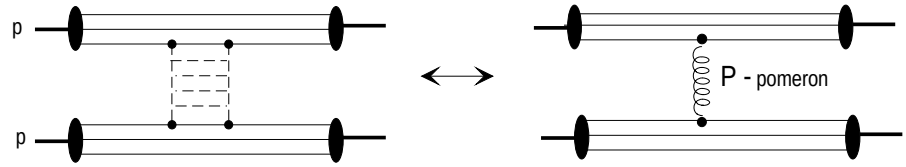

Fig. 1. The Pomeron diagrams for pp scattering in the traditional additive quark model

energy $s_{h_1h_2}$ will be defined more precisely below ((9)). $G_{h_i}(t)$ is the form factor of the hadron h_i; it takes into account a redistribution of momenta of the quarks inside a hadron after the interaction of one of them with the Pomeron (each system of quarks should be preserved, after the interaction, as a hadron of the same kind). It is clear that $G_{\mathcal{P}}^{(h_1)}(0) = G_{\mathcal{P}}^{(h_2)}(0) = 1$ at $t = 0$. In what follows, we apply the traditional and the modified AQM to describe the total cross sections

$$\sigma_{\rm tot}(s) = 8\pi {\rm Im}\, A(s,0) \tag{2}$$

and the ratios of the real to the imaginary forward amplitudes

$$\rho(s) = \frac{{\rm Re}A(s,0)}{{\rm Im}\, A(s,0)}. \tag{3}$$

For the Pomeron contribution to the quark–quark scattering, we will consider two schemes. The first one is the supercritical Pomeron (SCP), a Pomeron with an intercept larger than one; this is a variant of the Donnachie–Landshoff Pomeron (DLP)[13], but with a constant term added to reflect preasymptotic properties. This term is just a simple pole in the complex angular momentum plane j with unit intercept

$$A_{\mathcal{P}}^{(qq)}(s,0) = {\rm i}g_1^2[-\zeta + (-{\rm i}s/s_0)^{\alpha_{\mathcal{P}}(0)-1}]\ , \tag{4}$$

where $s_0 = 1\,{\rm GeV}^2$. The second model is the dipole Pomeron (DP) model (see, for instance [14]), corresponding to the sum of a simple pole and a double j pole with unit intercepts

$$A_{\mathcal{P}}^{(qq)}(s,0) = {\rm i}g_1^2[-\zeta + \ln(-{\rm i}s/s_0)]\ . \tag{5}$$

In the previous expressions, the parameter ζ is expected to be positive (from the fits to hadronic and γp cross sections [15–17]). As shown in [16], the Pomeron contribution at $t \neq 0$ is more complicated than (1) because each term in (4) and (5) should be multiplied by an *a priori* different vertex function $G(t)$. Thus, at $t \neq 0$, (1) must be rewritten as

$$A_{\mathcal{P}}^{(h_1h_2)}(s,t) = n_1n_2P_{h_1}P_{h_2}\sum_{i=1,2} A_{\mathcal{P}i}^{(qq)}(s_{h_1h_2},t)G_{\mathcal{P}i}^{(h_1)}(t)G_{\mathcal{P}i}^{(h_2)}(t), \tag{6}$$

where, generalizing (4) and (5),

$$\begin{aligned} A_{\mathcal{P}1}^{qq}(s,t) &= -{\rm i}g_1^2\zeta(-{\rm i}s/s_0)^{\tilde\alpha_{\mathcal{P}}(t)-1}, \\ A_{\mathcal{P}2}^{qq}(s,t) &= {\rm i}g_1^2 L(s,t), \quad \tilde\alpha_{\mathcal{P}}(0) = 1 \end{aligned} \tag{7}$$

and

$$\begin{aligned} L(s,t) &= (-{\rm i}s/s_0)^{\alpha_{\mathcal{P}}(t)-1}, \\ \alpha_{\mathcal{P}}(0) &> 1 \qquad \text{for SCP}, \end{aligned} \tag{8}$$

$$\begin{aligned} L(s,t) &= \ln(-{\rm i}s/s_0)(-{\rm i}s/s_0)^{\alpha_{\mathcal{P}}(t)-1}, \\ \alpha_{\mathcal{P}}(0) &= 1 \qquad \text{for DP}\ . \end{aligned} \tag{8$'$}$$

Generally speaking, the trajectories $\alpha_{\mathcal{P}}(t)$ and $\tilde\alpha_{\mathcal{P}}(t)$ can differ not only by their intercepts but also by their slopes. At high energy, in the center-of-mass system, each hadron has the energy $\sqrt{s}/2$ and, according to the AQM, each quark inside the hadron h_i has the energy $(\sqrt{s}/2)/n_i$ (if n_i is the number of quarks comprised in the hadron h_i). Thus, the energy of each pair of quarks (one from the hadron h_1 and the other from the hadron h_2) is

$$s_{h_1h_2} = \left(\frac{\frac{\sqrt{s}}{2}}{n_1} + \frac{\frac{\sqrt{s}}{2}}{n_2}\right)^2 - \left(\frac{\frac{\sqrt{s}}{2}}{n_1} - \frac{\frac{\sqrt{s}}{2}}{n_2}\right)^2 = \frac{s}{n_1n_2}. \tag{9}$$

There are nine (3×3) similar diagrams in pp scattering, contributing to the corresponding amplitudes

$$A_{\mathcal{P}i}^{(pp)}(s,t) = 9P_p^2\, A_{\mathcal{P}i}^{(qq)}(s/9,t)(G_{\mathcal{P}i}^{p}(t))^2, \qquad i = 1,2\ . \tag{10}$$

Considering also elastic πp scattering with 3×2 diagrams, one can write

$$A_{\mathcal{P}i}^{(\pi p)}(s,t) = 6P_pP_\pi\, A_{\mathcal{P}i}^{(qq)}(s/6,t)G_{\mathcal{P}i}^{p}(t)G_{\mathcal{P}i}^{\pi}(t), \quad i = 1,2. \tag{11}$$

Let us focus now on γ-induced processes, for which the main Pomeron contributions (in the AQM) are shown in Fig. 2.

The simplest approximation that describes the γp elastic scattering as due to the Pomeron is

$$A_{\mathcal{P}i}^{(\gamma p)}(s,t) = 6\alpha P_p\, A_{\mathcal{P}i}^{(qq)}(s/6,t)G_{\mathcal{P}i}^{p}(t)G_{\mathcal{P}i}^{\gamma}(t), \quad i = 1,2\ , \tag{12}$$

where $\alpha = {\rm e}^2/4\pi \approx 1/137$ is the fine-structure constant. (12) takes into account the $\gamma q\bar q$ vertices in the $q\bar q$ loop at the upper block of the diagram in Fig. 2a. Similarly, the relevant $\gamma\gamma$ amplitude (Fig. 2b) has the form

$$A_{\mathcal{P}i}^{(\gamma\gamma)}(s,t) = 4\alpha^2\, A_{\mathcal{P}i}^{(qq)}(s/4,t)(G_{\mathcal{P}i}^{\gamma}(t))^2, \quad i = 1,2\ . \tag{13}$$

It is more realistic, however, to consider a different picture for γp and $\gamma\gamma$ diagrams. In accordance with the vector meson dominance (VDM) model, the photon is transformed into a vector meson, which, after interacting with the Pomeron, comes back to a photon state. Thus we replace α with P_γ in (12, 13), where $\sqrt{P_\gamma}$ describes the transition of a γ into a pair $q\bar q$ (for instance, via a vector meson).

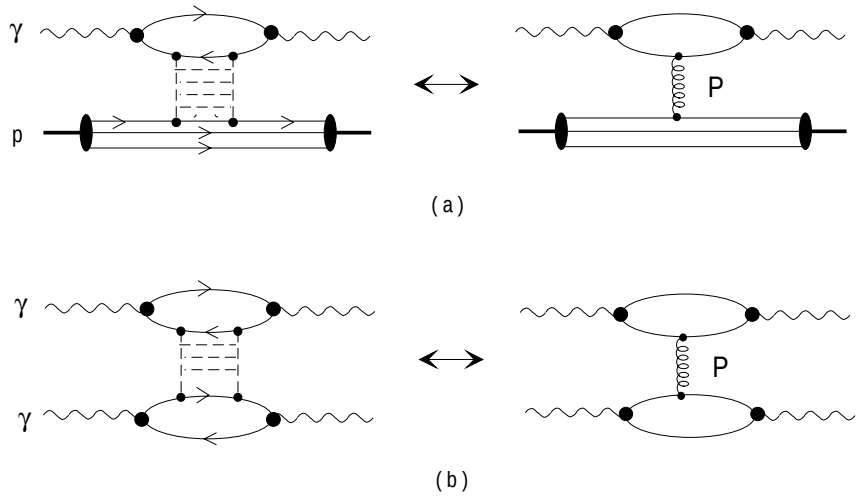

Fig. 2a,b. The Pomeron diagrams for (**a**) γp and (**b**) $\gamma\gamma$ scattering in the conventional AQM

2.2 Secondary Reggeons

At the presently attainable (subasymptotic) squared energy s, besides the Pomeron's contribution, one should retain also the contribution of other Reggeons (f, ρ, ω, etc.) to the elastic amplitudes. It is usually assumed that they are added to the Pomeron, so that the amplitude becomes

$$A^{(h_1h_2)}(s,t) = A_{\mathcal{P}}^{(h_1h_2)}(s,t) + n_1n_2P_{h_1}P_{h_2}\sum_R A_R^{(qq)}(s_{h_1h_2},t)G_R^{(h_1)}(t)G_R^{(h_2)}(t), \quad (14)$$

where the Pomeron amplitude is detailed in the preceding section, and the sum runs over all Reggeons (R) contributing to the given process. In what follows, we will consider pp, πp, γp and $\gamma\gamma$ scattering at $\sqrt{s} \geq 4\,\mathrm{GeV}$ and $t = 0$. Therefore, only f and ω will contribute to $p^{\mp}p$ processes (here and in what follows, $p^- \equiv \bar{p}$, $p^+ \equiv p$), f and ρ to $\pi^{\mp}p$, and f to γp and $\gamma\gamma$. For the secondary Reggeons, we take the standard forms

$$A_f^{(qq)}(s,t) = \mathrm{i}g_f^2\Big(-\mathrm{i}s/s_0\Big)^{\alpha_f(t)-1}, \quad (15)$$

$$A_\omega^{(qq)}(s,t) = g_\omega^2\Big(-\mathrm{i}s/s_0\Big)^{\alpha_\omega(t)-1}, \quad (16)$$

$$A_\rho^{(qq)}(s,t) = g_\rho^2\Big(-\mathrm{i}s/s_0\Big)^{\alpha_\rho(t)-1}. \quad (17)$$

2.3 Complete AQM amplitude

Collecting all the previous results, the relevant amplitudes at $t = 0$ [2] in the old AQM for the four cases under investigation are

$$A^{\binom{p\bar{p}}{pp}}(s,0) = 9P_p^2\left[A_{\mathcal{P}}^{(qq)}(s/9,0) + A_f^{(qq)}(s/9,0) \pm A_\omega^{(qq)}(s/9,0)\right], \quad (18)$$

$$A^{\binom{\pi^-p}{\pi^+p}}(s,0) = 6P_\pi P_p\left[A_{\mathcal{P}}^{(qq)}(s/9,0) \pm A_\rho^{(qq)}(s/6,0)\right], \quad (19)$$

$$A^{(\gamma p)}(s,0) = 6P_\gamma P_p\left[A_{\mathcal{P}}^{(qq)}(s/6,0) + A_f^{(qq)}(s/6,0)\right], \quad (20)$$

$$A^{(\gamma\gamma)}(s,0) = 4P_\gamma^2\left[A_{\mathcal{P}}^{(qq)}(s/4,0) + A_f^{(qq)}(s/4,0)\right] \quad (21)$$

where the Pomeron quark–quark amplitude $A_{\mathcal{P}}^{(qq)}$ is defined by (4) or (5), and the Reggeon quark–quark amplitudes $A_R^{(qq)}$ are given in (15)–(17).

The details of the fit with the conventional AQM model are given in Sect. 4. Here we note only that the *quality* of the fit is not so good (χ^2/d.o.f. ≈ 3) where d.o.f. stands for *degrees of freedom*.

3 Modification of the additive quark model

3.1 Pomeron

In the spirit of the QCD-like picture, we can say that the Pomeron has at least four gluonic edges coupled with quark lines. However, we would like to stress here that, as is well known, a soft Pomeron (dominating the elastic scattering amplitudes) is not just a two-gluon state (an approximation used, for example, in [7,8]). Similarly, it is not just a gluonic ladder (another approximation also used rather often), and, perhaps most importantly, it can not yet be calculated within QCD. Finally, it is not even a simple Regge pole, leading either to a constant total cross section or to a violation of the Froissart–Martin unitarity bound. At present, only phenomenological models of the Pomeron can successfully describe, without at least a rough violation of unitarity, the available data on the various cross sections in a soft kinematic region.

Therefore, in spite of the often-mentioned analogy between the Pomeron and a gluonic ladder, the soft Pomeron diagrams at the right of Fig. 2a and 2b are not just the ladder diagrams shown on the left of each figure. The

[2] This is all we need for total cross sections.

latter, in fact, assume that each edge of the gluonic ladder of the Pomeron couples to the hadron, via lines of individual quarks only. Besides the diagrams of Figs. 1 and 2, additional terms may contribute to the amplitudes. They include, for instance, diagrams in which the Pomeron line is coupled with two quark lines rather than with one line only, leading to a modified additive quark model (MAQM). Examples of such diagrams are typified in Fig. 3. Notice, however, that the diagrams on the right-hand side of Fig. 3 are indeed much more complicated than the left-hand-side ladder diagrams; for instance, they take into account that a soft Pomeron can interact with a pair of quarks as a whole (not necessarily a diquark; all possible states of this pair of quarks, excluding the two separated quarks, have to be included, and are somehow "hidden" in this new coupling). These kinds of couplings were absent in the conventional AQM. Figure 3a exhibits *one* such new coupling, while *both* couplings are new in Fig. 3b. The left-hand-side diagrams of all figures are to be considered only as an indication of what should be the leading terms describing the actual couplings.

Lacking an adequate mathematical formalism to really *calculate* the soft Pomeron, we take a pragmatic attitude to simulate the effects of these more general couplings, and assume that the cheapest price to pay for this generalization is an additional coupling constant describing the vertex of a Pomeron with two quarks. This constant will have to be determined from the fit to the data, and can be considered as a measure of the deviation between the new counting rules and the old ones. We expect (and this is confirmed by fitting the data) that this constant is small, and we neglect the effect simulating the interaction of the Pomeron with three quarks as a whole.

In summary, our main assumption for the Pomeron is that there exists a coupling constant Pomeron (pair of quarks), which leads to new terms in the elastic amplitude. In what follows, we obtain the counting rules for these terms and determine from the experimental data a magnitude of the corrections to the traditional AQM amplitudes.

Taking into account all possible diagrams that can contribute to each case, we redefine the Pomeron contributions (10–13) as follows (once again, it is sufficient to write all amplitudes at $t = 0$ because our modification concerns the counting rules rather than the form of the amplitudes; a generalization to $t \neq 0$ is, however, immediate from the previous section):
The $p^{\mp}p$ interaction is

$$A_{\mathcal{P}}^{(pp)}(s,0) = 9P_p^2[A_{\mathcal{P}}^{(1)}(s/9,0)+2A_{\mathcal{P}}^{(2)}(2s/9,0)+A_{\mathcal{P}}^{(3)}(4s/9,0)], \quad (22)$$

the $\pi^{\mp}p$ interaction is

$$A_{\mathcal{P}}^{(\pi p)}(s,0) = 3P_\pi P_p[2A_{\mathcal{P}}^{(1)}(s/6,0)+3A_{\mathcal{P}}^{(2)}(s/3,0) +A_{\mathcal{P}}^{(3)}(2s/3,0)], \quad (23)$$

the γp interaction is

$$A_{\mathcal{P}}^{(\gamma p)}(s,0) = 3P_\gamma P_p[2A_{\mathcal{P}}^{(1)}(s/6,0)+3A_{\mathcal{P}}^{(2)}(s/3,0)+A_{\mathcal{P}}^{(3)}(2s/3,0)], \quad (24)$$

and the $\gamma\gamma$ interaction is

$$A_{\mathcal{P}}^{(\gamma\gamma)}(s,0) = P_\gamma^2[4A_{\mathcal{P}}^{(1)}(s/4,0)+4A_{\mathcal{P}}^{(2)}(s/2,0)+A_{\mathcal{P}}^{(3)}(s,0)], \quad (25)$$

where

$$A_{\mathcal{P}}^{(1)}(s,0) = \mathrm{i}[-\eta_1^2 + g_1^2 L(s)], \quad (26)$$

is the Pomeron contribution to the amplitude in the old AQM, in which η_1^2 replaces the term ζg_1^2, (we mentioned already that, when the data are fitted, ζ turns out to be positive). Two new contributions appear in each of the above expressions, because the new coupling constants g_2, η_2 simulate the interaction of the Pomeron with a pair of quarks (they give the corrections which we call MAQM):

$$A_{\mathcal{P}}^{(2)}(s,0) = \mathrm{i}[-\eta_1\eta_2 + g_1 g_2 L(s)], \quad (27)$$

$$A_{\mathcal{P}}^{(3)}(s,0) = \mathrm{i}[-\eta_2^2 + g_2^2 L(s)] \; . \quad (28)$$

Here $L(s) = (-\mathrm{i}s/s_t)^{\alpha_{\mathcal{P}}(0)-1}$ in the SCP model, $L(s) = \ln(-\mathrm{i}s/s_0)$ in the DP model, and η_1, η_2 are constants. The numerical coefficient in front of each term of the amplitudes (22)–(25) is just the number of possible diagrams contributing to each of the various vertices.

As previously discussed, each Pomeron term $A_{\mathcal{P}}^{(i)}(s,0)$, $i = 1, 2, 3$, is the sum of two contributions. The first corresponds to a double j pole (with couplings g_1, g_2 describing the vertices with one and two quarks, respectively, as indicated in Fig. 1 and Fig. 3) and the second corresponds to a simple pole (with couplings η_1 and η_2).

The negative sign in front of the η in (26)–(28) simply reflects the observation that this is required by the fits to the data.

Comparing the new formulation we have to the AQM, we see we have four parameters to determine η_1, η_2 and g_1, g_2. The available data, however, are not sufficient to determine four coupling constants (g_k, η_k); for this reason we consider the simpler case in which

$$\eta_1^2/g_1^2 = \eta_2^2/g_2^2 = \zeta.$$

As follows from unitarity, the total cross sections for nn, πn and $\pi\pi$ interactions (by cross section nn and πn, we mean $\sigma_{nn} = (\sigma_{pp} + \sigma_{\bar{p}p})/2$ and $\sigma_{\pi n} = (\sigma_{\pi^+ p} + \sigma_{\pi^- p})/2$) should satisfy the asymptotic factorization relation [18],

$$\sigma_{\pi n}^2 = \sigma_{\pi\pi}\sigma_{nn}.$$

One can check that this relation holds also in the MAQM if the constant terms in (26)–(28) are neglected. But the well-known relation $\sigma_{\pi n}/\sigma_{nn} = 3/2$ does not hold exactly in the MAQM. For the dipole Pomeron ($L(s) = \ln(-\mathrm{i}s/s_0)$), this is modified into

$$\sigma_{\pi n}/\sigma_{nn} = \sigma_{\pi\pi}/\sigma_{\pi n} \approx \frac{2P_\pi}{3P_p}\left(1 - \frac{1}{2}\frac{g_1}{g_2}\right),$$

if $g_1/g_2 \ll 1$, as is expected (this is confirmed by the data; see below). The same relations are valid (under the replacement $\pi \to \gamma$ in the indices) for the nn, γn and $\gamma\gamma$ processes.

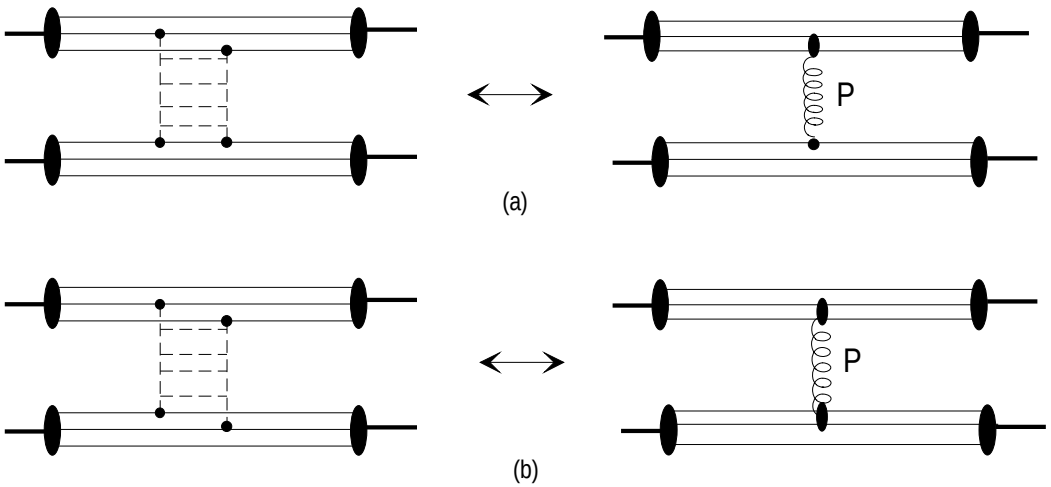

Fig. 3a,b. New Pomeron diagrams in the MAQM (examples): (**a**) only one Pomeron vertex is new; (**b**) both vertices are new

3.2 Secondary Reggeons.

In this section we discuss why the modifications of the counting rules for secondary Reggeons are different from those for the Pomeron, which have a different quark–gluonic structure. As already noted, this difference is usually ignored in the AQM.

While the Pomeron is mostly a gluonic state which can be coupled with any quark, independently of its flavor, the Reggeons are, essentially, $q\bar{q}$ states (see Fig. 4). The diagrammatic structure of the f Reggeon (as well as other Reggeons with vacuum quantum numbers) which, being neutral, is a mixing of $u\bar{u}$ and $d\bar{d}$ (not of $u\bar{d}$ and $d\bar{u}$) states,[3] is shown in Fig. 4.

Thus, in the pp diagram we show that the f Reggeon can couple only to quarks with identical flavor. There are four diagrams which show the f Reggeon coupling to u quarks, and one which shows its coupling to d quarks. This totals to five f Reggeon diagrams of pp scattering, compared to nine diagrams for the Pomeron and nine for the f Reggeon in the old AQM. We obtain

$$A_f^{(pp)}(s,0) = 5P_p^2 A_f^{(qq)}(s/9,0). \tag{29}$$

Similarly, for the πp diagrams we have

$$A_f^{(\pi p)}(s,0) = 3P_\pi P_p A_f^{(qq)}(s/6,0). \tag{30}$$

The same couplings apply to γp diagrams. The upper loop shown in Fig. 4b can contain either $u\bar{u}$ or $d\bar{d}$ quarks, with 1/2 probability for each case. Therefore, there are $2\times 2\times \frac{1}{2} = 2$ terms for the u loop, and $2\times\frac{1}{2}=1$ term for the d loop, leading to

$$A_f^{(\gamma p)}(s,0) = 3P_\gamma P_p A_f^{(qq)}(s/6,0). \tag{31}$$

Performing a similar counting for the $\gamma\gamma$ amplitude, we obtain

$$A_f^{(\gamma\gamma)}(s,0) = 2P_\gamma^2 A_f^{(qq)}(s/4,0). \tag{32}$$

[3] We ignore here the small contribution of other $q\bar{q}$ states to the f meson and, consequently, to the f Reggeon.

The crossing-odd ω Reggeon contributes only to the pp and $\bar{p}p$ amplitudes, and we have

$$A_\omega^{(pp)}(s,0) = 5P_p^2 A_\omega^{(qq)}(s/9,0). \tag{33}$$

Similarly, counting the ρ contribution to the $\pi^{\mp}p$ amplitudes gives

$$A_\rho^{(pp)}(s,0) = 3P_p^2 A_\rho^{(qq)}(s/6,0). \tag{34}$$

Strictly speaking, we should consider another kind of contribution since, in addition to the previous coupling of two quark lines having the same flavor (uu or dd), we could also have a coupling of two quark lines that have different flavors (ud), because all secondary Reggeons with vacuum quantum numbers are mixed states of $u\bar{u}$ and $d\bar{d}$ (we neglect harder flavors).

Once again, lacking the tools to actually perform the calculation, we resort to describing the transition from a $u\bar{u}$ to a $d\bar{d}$ state, through just one new additional constant (see Fig. 5), and we assume, for simplicity, that this new contribution is given by multiplying the old Reggeon term R by a constant λ_R. Note, however, that the counting rules for these new terms are different from those which couple identical quarks.

Putting everything together, the complete f Reggeon contribution to the amplitudes is now the following:
The pp interaction is

$$\begin{aligned} A_f^{(pp)}(s,0) &= P_p^2[5A_{f1}^{(qq)}(s/9,0) + 4A_{f2}^{(qq)}(s/9,0)] \\ &= P_p^2(5+4\lambda_f)A_f^{(qq)}(s/9,0), \end{aligned} \tag{35}$$

the πp interaction is

$$\begin{aligned} A_f^{(\pi p)}(s,0) &= 3P_\pi P_p[A_{f1}^{(qq)}(s/6,0) + A_{f2}^{(qq)}(s/6,0)] \\ &= 3P_\pi P_p(1+\lambda_f)A_f^{(qq)}(s/6,0), \end{aligned} \tag{36}$$

the γp interaction is

$$\begin{aligned} A_f^{(\gamma p)}(s,0) &= 3P_\gamma P_p[A_{f1}^{(qq)}(s/6,0) + A_{f2}^{(qq)}(s/6,0)] \\ &= 3P_\gamma P_p(1+\lambda_f)A_f^{(qq)}(s/6,0), \end{aligned} \tag{37}$$

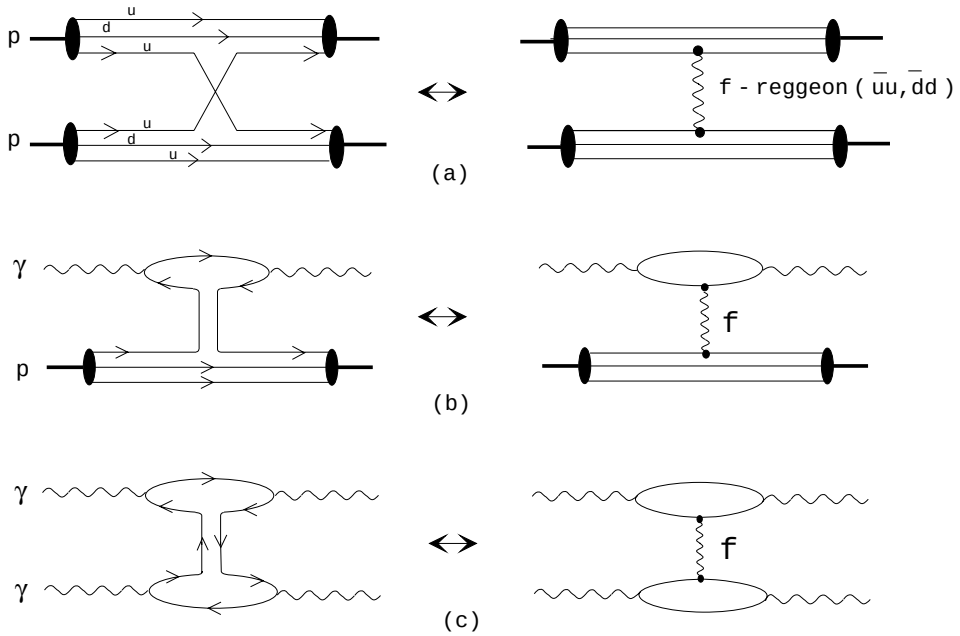

Fig. 4a–c. The f Reggeon diagrams for (**a**) pp, (**b**) γp and (**c**) $\gamma\gamma$ scattering. The left diagrams give an example of the quark–gluonic content of the f Reggeon and visualize the counting rules for the f contribution

Fig. 5. Mixing of $u\bar{u}$ and $d\bar{d}$ states in a secondary Reggeon

and the $\gamma\gamma$ interaction is

$$A_f^{(\gamma\gamma)}(s,0) = 2P_\gamma^2[A_{f1}^{(qq)}(s/4,0) + A_{f2}^{(qq)}(s/4,0)] = 2P_\gamma^2(1+\lambda_f)A_{f1}^{(qq)}(s/4,0), \quad (38)$$

where

$$A_{f1}^{(qq)}(s,0) \equiv A_f^{(qq)}(s,0)$$

and

$$A_{f2}^{(qq)}(s,0) \equiv \lambda_f A_f^{(qq)}(s,0)\ .$$

The value of λ_f should be determined from a fit to the experimental data. Note that if $\lambda_f = 1$, one must go back to the old counting rules for the f Reggeon. The ω and ρ Reggeon contributions are easily derived from the above expressions. It should be noted that the counting rules for these Reggeons are unimportant in our fit, because we consider one by one the processes to which they contribute. Namely, ω contributes only to pp, and ρ contributes only to πp amplitudes. Thus, it is sufficient to write them in the old AQM form, if only $pp, \pi p, \gamma p$ and $\gamma\gamma$ cross sections are considered.

3.3 Complete MAQM amplitudes

Summarizing the results of the new counting rules, the final expressions for the $t = 0$ amplitudes of the reactions under investigation in the MAQM are:

1. the pp and $\bar{p}p$ (or $p^{\mp}p$) amplitudes:

$$A^{p^{\mp}p}(s,0) = P_p^2\{9[A_{\mathcal{P}}^{(1)}(s/9,0) + 2A_{\mathcal{P}}^{(2)}(2s/9,0) + A_{\mathcal{P}}^{(3)}(4s/9,0)] + (5+4\lambda_f)A_f(s/9,0) \pm 9A_\omega(s/9,0)\}; \quad (39)$$

2. $\pi^- p$ and $\pi^+ p$ amplitudes:

$$A^{\pi^{\mp}p}(s,0) = P_\pi P_p\{3[2A_{\mathcal{P}}^{(1)}(s/6,0) + 3A_{\mathcal{P}}^{(2)}(s/3,0) + A_{\mathcal{P}}^{(3)}(2s/3,0)] + 3(1+\lambda_f)A_f(s/6,0) \pm 6A_\rho(s/6,0)\}; \quad \text{and} \quad (40)$$

3. the γp amplitude:

$$A^{\gamma p}(s,0) = P_\gamma P_p\{3[2A_{\mathcal{P}}^{(1)}(s/6,0) + 3A_{\mathcal{P}}^{(2)}(s/3,0) + A_{\mathcal{P}}^{(3)}(2s/3,0)] + 3(1+\lambda_f)A_f(s/6,0)\}; \quad (41)$$

4. and the $\gamma\gamma$ amplitude:

$$A^{\gamma\gamma}(s,0) = P_\gamma^2\{4A_{\mathcal{P}}^{(1)}(s/4,0) + 4A_{\mathcal{P}}^{(2)}(s/2,0) + A_{\mathcal{P}}^{(3)}(s,0) + 2(1+\lambda_f)A_f(s/4,0)\}. \quad (42)$$

4 Comparison with the data

Both models (the old AQM and MAQM) have been fitted to the experimental data [9,10,19,20] at $\sqrt{s} \geq 4\,\text{GeV}$ (the total is 434 points):

Observable	σ_{pp}	$\sigma_{\bar{p}p}$	$\sigma_{\pi^- p}$	$\sigma_{\pi^+ p}$	$\sigma_{\gamma p}$	$\sigma_{\gamma\gamma}$	ρ_{pp}	$\rho_{\bar{p}p}$
N of points	85	51	49	83	68	17	64	17

In our data set, we do not include a few points on $\rho^{\pi^\pm p}$ because of their large errors. This does not lead to any noticeable change in the values of parameters or in the behavior of the curves. Without any loss of generality, we can take $P_p = 1$ in the previous equations, since this acts as an overall multiplicative parameter in the fit.

We compare three possibilities for the Pomeron:

(a) DLP : supercritical Pomeron with $\zeta = 0$ in (4) (this is close to the Pomeron of [13]),
(b) SCP : supercritical Pomeron with free ζ, and
(c) DP : dipole Pomeron with $\alpha_{\mathcal{P}}(0) = 1$.

4.1 The old AQM

The descriptions of these data in the old AQM models with the different Pomerons mentioned above are comparable to each other; the χ^2 in cases (b) and (c), χ^2/d.o.f. $\approx$ 3.04, is very close to that in case (a), χ^2/d.o.f. $\approx$ 3.09. It is interesting to note, nevertheless, that if the parameter ζ is allowed to be free, the intercept of the supercritical Pomeron tends to 1 and the other parameters approach those obtained in the dipole Pomeron model. The same situation was observed in [15], where these models were compared with all the data on the meson–nucleon and nucleon–nucleon cross sections and ratios of the real to the imaginary parts of the amplitudes. We will come back to these questions below when discussing the MAQM. In Figs. 6–9 we present the curves (the dashed/dotted lines) corresponding to the dipole Pomeron (case (c)). The curves for both variants of SCP are indistinguishable by eye from the DP curves.

Table 1. The values of parameters obtained in MAQM for three variants of Pomeron

Parameters	SCP, $\zeta = 0$	SCP, $\zeta \neq 0$	DP
g_1 (GeV^{-1})	0.583	13.346	0.317
g_2 (GeV^{-1})	-0.079	-0.826	-0.024
$\alpha_{\mathcal{P}}(0)$	1.101	1.0005	1.0 (fixed)
ζ	0.0 (fixed)	1.003	3.399
P_p	1.0 (fixed)	1.0 (fixed)	1.0 (fixed)
P_π	0.848	0.925	0.919
P_γ	0.0041	0.0044	0.0044
g_f (GeV^{-1})	0.822	1.120	1.112
$\alpha_f(0)$	0.661	0.803	0.810
λ_f	0.094	0.343	0.439
g_ω (GeV^{-1})	0.396	0.395	0.395
$\alpha_\omega(0)$	0.403	0.418	0.421
g_ρ (GeV^{-1})	0.230	0.221	0.222
$\alpha_\rho(0)$	0.592	0.586	0.587
χ^2/d.o.f.	2.025	1.784	1.780

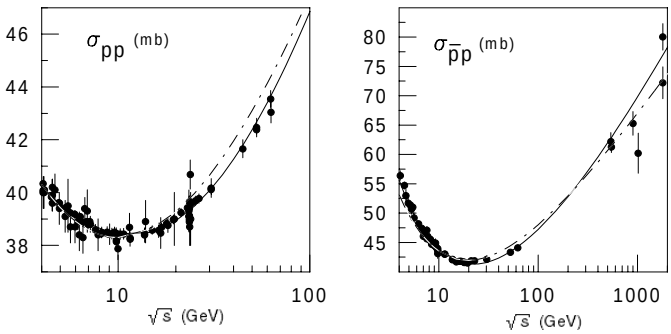

Fig. 6. Total pp and $\bar{p}p$ cross sections described in the old (dashed/dotted lines) and modified (solid lines) AQM with the dipole Pomeron

4.2 The modified AQM

The same set of data is now used to perform the fit within the MAQM. The values of the free parameters for the three models of Pomeron considered are given in Table 1. It is evident that the MAQM leads to a better description of the data: The χ^2/d.o.f. decreases from 3.04 to 1.78 for cases (b) and (c), and to 2.03 for case (a). The behavior of σ_{tot} and ρ is shown in Figs. 6–9 by the solid curves (once again, we confine ourselves to plotting the curves for the case of the dipole Pomeron only). The improvement for all cross sections and $\rho^{p^\mp p}$ is quite visible.

We can clearly see, therefore, that the MAQM agrees with the data better than the old AQM does.

We also note that the supercritical Pomeron with an additional constant term (i.e., with $\zeta = \eta_1^2/g_1 = \eta_2^2/g_2 \neq 0$ in (26)–(28) is very close to the dipole Pomeron. As a matter of fact, given the small value of $\epsilon \equiv \alpha_{\mathcal{P}}(0) - 1$ obtained from the fit (see Table 1), $\epsilon \approx 0.0005$, one can write the supercritical Pomeron contribution, for instance to the pp amplitude, in a form indistinguishable, in practice, from the dipole Pomeron case:

$$A_{\mathcal{P}}^{pp} = \mathrm{i}g_1^2[-\zeta + (-\mathrm{i}s/s_0)^\epsilon] \approx \mathrm{i}g_1^2[-\zeta + 1 + \epsilon \ln(-\mathrm{i}s/s_0)] = \mathrm{i}\tilde{g}_1^2[-\tilde{\zeta} + \ln(-\mathrm{i}s/s_0)],$$

where $\tilde{g}_1^2 = \epsilon g_1^2$, $\tilde{\zeta} = (\zeta - 1)/\epsilon$. From the parameters given in Table 1, we find $\tilde{g}_1 \approx 0.31$, $\tilde{\zeta} \approx 3.02$, which are close to the corresponding parameters of the dipole Pomeron. The parameters of the other Reggeons are also close to those obtained for the dipole Pomeron model.

From this point of view, we can say that the dipole Pomeron is preferable to the supercritical Pomeron. From the theoretical point of view, it will never violate the Froissart–Martin unitarity bound, and from the phenomenological point of view, it has one parameter fewer (because $\alpha_{\mathcal{P}}(0) = 1$).

Our analysis of the data does not support the conclusion drawn in [11] about $\sigma_{\mathrm{inel}}^{\gamma\gamma}$, in which it is claimed that the preliminary results of the OPAL Collaboration are doubtful and that the Vector Meson Dominance model

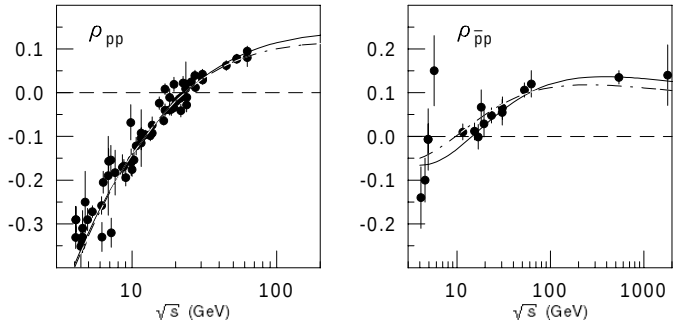

Fig. 7. The ratio of the real to the imaginary part of the forward amplitudes of pp and $\bar{p}p$ elastic scattering in the old (dashed/dotted lines) and modified (solid lines) AQM with the dipole Pomeron

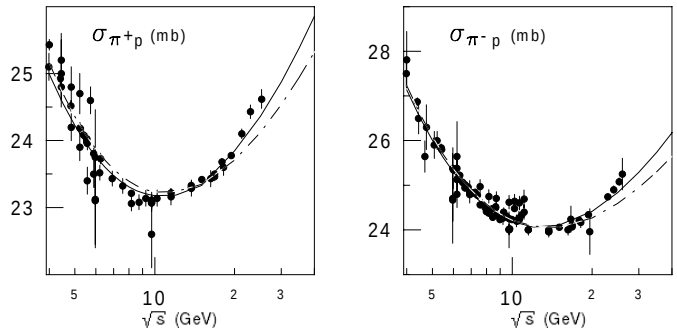

Fig. 8. Total $\pi^{\mp}p$ cross sections described in the old (dashed/dotted lines) and modified (solid lines) AQM with the dipole Pomeron

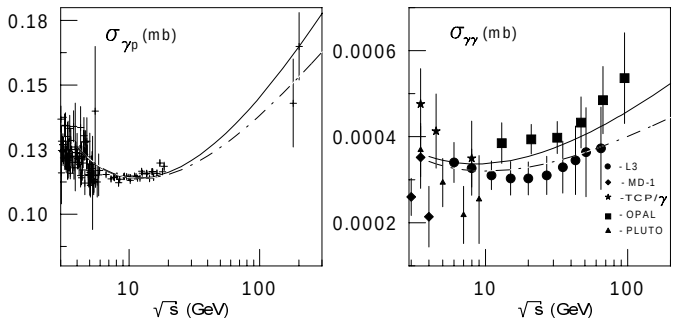

Fig. 9. Total γp and $\gamma\gamma$ cross sections described in the old (dashed/dotted lines) and modified (solid lines) AQM with the dipole Pomeron

(VMD) selects the L3 data[4]. One can see from Fig. 9 that the theoretical curve goes precisely between the data points of these two groups. Generally, we predict higher values of $\sigma^{\gamma p}$ and $\sigma^{\gamma\gamma}$ than those given in [11], but smaller than those obtained for these cross sections in the mini-jets model [21].

[4] The predictions of [11] are based on the counting rules of the old AQM, which should be modified the way we have described.

5 Conclusion

Our main result is the following. A better phenomenological account of the quark–gluonic content of Pomeron and f Reggeon leads to slightly modified counting rules for the quark–quark amplitudes when the hadron–hadron, photon–hadron and photon–photon amplitudes are constructed. The additional new Pomeron terms give approximately 10% of the whole Pomeron contribution, while for the f Reggeon, the new term contributes approximately 30% of the whole f Reggeon component. The important role of these terms is confirmed by the analysis of the data on the total cross sections of hadron- and photon-induced processes. They lead to a decrease of the χ^2/d.o.f. by approximately 40%, qualitatively improving the description of the data.

In conclusion, we have shown that the simple one-parameter modification of the Pomeron in the additive quark model, along with a careful counting of the contributing diagrams, leads to a quantitatively better fit of all available $t = 0$ data. This noticeable improvement gives us reason to believe that the MAQM will give a substantially better result when the model is applied outside $t = 0$. We plan to do this in the near future.

Acknowledgements. We gratefully acknowledge the financial support provided by the IN2P3 of France and by the INFN and the MURST of Italy. E. M. wishes also to thank the theory groups of the Universities of Lyon and Torino for their hospitality.

References

1. E.M. Levin, L.L. Frankfurt, Pisma ZhETP, **3**, 105 (1965)
2. H.J. Lipkin, F. Sheck, Phys. Rev. Lett. **16**, 71 (1966)
3. J.J.J. Kokkedee, L. Van Hove, Nuovo Cim. **42A**, 711 (1966)
4. J.J.J. Kokkedee, *The Quark model*, (W.A. Benjamin, Inc., New York, 1969)
5. V.V. Anisovich, Yu.M. Shabelsky, V.M. Shekhter, Nucl. Phys. **B133**, 477 (1978)
6. E.S. Martynov, in *Proceedings of the Workshop DIQUARKS II, Torino, Italy, 1992*
7. J.F. Gunion, D.E. Soper, Phys. Rev. **D15**, 2617 (1977)
8. E.M. Levin, M.G. Ryskin, Yad. Fiz. (Sov. Nucl. Phys.) **34**, 1114 (1981)
9. M. Derrick, et al., ZEUS Collaboration, Zeit. Phys. **C63**, 391 (1994); S. Aids, et al., H1 Collaboration, Zeit. Phys. **C69**, 27 (1995); Data for γp cross sections at low energies can be found, for instance, in the Durham Data Base (http://cpt1.dur.ac.uk/HEPDATA)
10. Ch. Berger, et al., PLUTO Collaboration, Phys. Lett. **B149**, 421 (1984); H. Aihara, et al., TCP/2γ Collaboration, Phys. Rev. **D41**, 2667 (1990); S.E. Baru, et al., MD-1 Collaboration, Zeit. Phys. **C53**, 219 (1992); M. Acciari, et al., L3 Collaboration, Phys. Lett. **B408**, 450 (1997); F. Wäckerle, "Total Hadronic Cross-section for Photon–Photon Interactions at LEP", (Preprint Freiburg–EHEP-97-17, 1997)

11. M.M. Block, et al., Phys. Rev. **D58**, 17503 (1998, hep-ph/9809403)
12. A. Donnachie, R.G. Dosch, M. Rueter, Phys. Rev. D **59**, 074011 (1999), hep-ph/9810206, 1998
13. A. Donnachie, P. Landshoff, Phys. Lett. **B296**, 227 (1992)
14. L.L. Jenkovszky, Fortschr. Phys. **34**, 702 (1986); M. Bertini, et al., Rivista Nuovo Cim. **19**, 1 (1996)
15. P. Desgrolard, et al., Nuovo Cim. **107A**, 637 (1994)
16. P. Desgrolard, A.I. Lengyel, E.S. Martynov, Nuovo Cim. **110A**, 251 (1997)
17. P. Desgrolard, A.I. Lengyel, E.S. Martynov, Eur. Phys. J. C **7**, 655 (1999)
18. See, for example, P.D.B. Collins, *An Introduction to Regge Theory and High Energy Physics* (Cambridge University Press, Cambridge 1977)
19. For pp and $\bar{p}p$ data on $\sigma_{\rm tot}$ and ρ see, for example, S.M. Pruss, in *Frontiers in Strong Interactions, VII Blois Workshop on Elastic and Diffractive Scattering, Chateau de Blois, France, June 1995*, edited by P. Chiappetta, M. Haguenauer, J. Tran Thanh Van (Editions Frontières 1996), p. 3, and references therein; Durham Data Base (http://cpt1.dur.ac.uk/HEPDATA)
20. Data on πp total cross sections can be found in the Durham Data Base (http://cpt1.dur.ac.uk/HEPDATA)
21. A. Corsetti, R.M. Godbole, G. Pancheri, Phys. Lett. **B435**, 441 (1998)